NUCL SCI TECH (2019) 30:43
https://doi.org/10.1007/s41365-019-0572-8

Impact parameter dependence of the yield ratios of light particles as a probe of neutron skin

Ting-Zhi Yan[1] · **Shan Li**[1]

Received: 5 November 2018 / Revised: 29 December 2018 / Accepted: 3 January 2019 / Published online: 13 February 2019

Abstract The yield ratios of neutron/proton ($R(n/p)$) and ^{3}H/^{3}He ($R(t/^3\mathrm{He})$) with reduced rapidity from 0 to 0.5 are investigated for 50 MeV/u $^{42,44,46,48,50,52,54,56}\mathrm{Ca} + {}^{40}\mathrm{Ca}$. This was conducted at whole reduced impact parameters using the isospin-dependent quantum-molecular-dynamics model in which the initial neutron and proton densities are sampled within the Skyrme–Hartree–Fock model, using which the neutron skin thickness (ΔR_{np}) is determined for different neutron-rich Ca isotopes. The results show that both $R(n/p)$ and $R(t/^3\mathrm{He})$ have strong linear correlations with ΔR_{np} of different Ca isotopic projectiles from five different centralities. It is suggested that $R(n/p)$ and $R(t/^3\mathrm{He})$, from the same centrality, could be treated as possible experimental observables to extract the neutron skin or halo thickness for neutron-rich isotopic nuclei, including the nuclei near the neutron drip line.

Keywords Yield ratio · Neutron skin thickness · Isospin-dependent quantum-molecular-dynamics

This work was supported by the National Natural Science Foundation of China (No. 11405025).

✉ Ting-Zhi Yan
ytz0110@163.com

1 School of Energy and Power Engineering, Northeast Electric Power University, Jilin 132012, China

1 Introduction

The equation of state (EOS) of neutron-rich nuclear matter, especially the symmetry energy term, is of great importance in nuclear physics and nuclear astrophysics [1, 2]. Neutron-rich nuclei-induced reactions provide an opportunity to study the symmetry energy term in the EOS of dense neutron-rich matter [3–6]. Several experimental observables have been proven to be sensitive to nuclear symmetry energy, including the neutron/proton ratio [7–9], isospin diffusion [10, 11], isospin fractionation and isoscaling [12–14], differential elliptic flow [15, 16], interaction cross section, charge-changing cross section [17], nucleon–nucleon momentum-correlation function [18], and α-decay half-life [19]. Among these observables, the neutron/proton ratio is probably the best probe for studying symmetry energy because symmetry potentials act directly on nucleons and thus affect the yield of free nucleons in heavy-ion reactions. The determination of the exact symmetry energy depends on the proton and neutron density distributions; hence, the proton and neutron density distributions are required with high accuracy. The proton density distribution can be determined to a high degree of accuracy by electromagnetic interactions such as those in electron scattering experiments, while the neutron density distribution is relatively poorly obtained from hadron–nucleus interactions because of the complexity of the strong interactions between nucleons. Neutron skin thickness is commonly used to refer to the difference between the neutron and the proton root-mean-square radii: $\Delta R_{\mathrm{np}} = \langle r^2\rangle_{\mathrm{n}}^{1/2} - \langle r^2\rangle_{\mathrm{p}}^{1/2}$. The yield ratio of neutron to proton ($R(n/p)$) [20], and the yield ratio of triton to ^{3}He ($R(t/^3\mathrm{He})$) [21] at projectile-like rapidity and large centrality have been found to have a strong linear correlation with neutron skin thickness ΔR_{np} for a certain neutron-rich Ca projectile. In their work [20, 21], the neutron and proton density distributions and the different ΔR_{np} are obtained by adjusting the diffuseness parameter in the droplet model for a Ca isotope, and these distributions are used for the phase initialization of a Ca projectile. Different yield ratios are then obtained from the isospin-dependent quantum-molecular-dynamics (IQMD) model simulated reaction events with different projectile initialized phase space. Thus, $R(n/p)$ and $R(t/^3\mathrm{He})$ are suggested as experimental observables to extract ΔR_{np} for neutron-rich nuclei. In this work, we use the SkM* parameters in Skyrme–Hartree–Fock (SHF) model for different neutron-rich Ca isotopes to obtain the ΔR_{np}, and the neutron and proton density distributions that are used to generate the projectile initialization phase space for the IQMD model. Moreover, the yield ratios of neutron to proton, and triton to ^{3}He in midrapidity from wide Ca isotope-induced reactions $^{42,44,46,48,50,52,54,56}\mathrm{Ca} + {}^{40}\mathrm{Ca}$ at 50 MeV/u are explored, and the reduced impact parameter dependence of the relationship between these yield ratios and neutron skin thickness is investigated.

2 Theoretical descriptions

The quantum-molecular-dynamics (QMD) model is a successful many-body theory that can explicitly describe the state of the reaction system and can represent the time evolution of the colliding system quite well from intermediate to relativistic energies. Thus, it can provide valuable information about both the collision dynamics and the fragmentation process. As a dynamical model, it mainly consists of several components: initialization of the projectile and the target nucleons, nucleons' propagation in the mean field, nucleon–nucleon collisions in nuclear medium, and Pauli blocking. A detailed review of the QMD model can be seen in Ref. [22]. The IQMD model is based on the above theory combined with isospin effect on the mean field, nucleon–nucleon collisions, and Pauli blocking [23, 24].

In the IQMD model, each nucleon is represented by a Gaussian wave packet:

$$\psi_i(\vec{r},t) = \frac{1}{(2\pi L)^{3/4}} \exp\left[-\frac{(\vec{r}-\vec{r}_i(t))^2}{4L}\right] \exp\left[-\frac{i\vec{r}\cdot\vec{p}_i(t)}{\hbar}\right] \quad (1)$$

where $\vec{r}_i(t)$ and $\vec{p}_i(t)$ are the ith wave pocket in the coordinate and momentum space, L is the wave pocket width, and $L = 2.16\,\mathrm{fm}^2$) is used in this study. The nuclear mean-field potential used in the IQMD model can be parameterized as the following [23, 24]:

$$\begin{aligned} U(\rho,\tau_z) = {} & \alpha\left(\frac{\rho}{\rho_0}\right) + \beta\left(\frac{\rho}{\rho_0}\right)^{\gamma} + \frac{1}{2}(1-\tau_z)V_{\mathrm{c}} \\ & + C_{\mathrm{sym}}\frac{(\rho_{\mathrm{n}}-\rho_{\mathrm{p}})}{\rho_0}\tau_z + U^{\mathrm{Yuk}} \end{aligned} \quad (2)$$

where ρ_0 is the normal nuclear matter density ($0.16\,\mathrm{fm}^{-3}$); ρ and ρ_{p}, ρ_{n} are the total proton and neutron densities, respectively; τ_z is the zth constituent of the isospin degree of freedom, which equals 1 or -1 for neutrons or protons, respectively. The different parameters α, β, and γ represent the different nuclear equations of state. C_{sym} is the symmetry energy strength due to the asymmetry of neutrons and protons in a nucleus. In this study, we adopt $\alpha = -356\,\mathrm{MeV}$, $\beta = 303\,\mathrm{MeV}$, and $\gamma = 1.17$ which corresponds to the so-called soft EOS with an incompressibility of $K = 200\,\mathrm{MeV}$ and $C_{\mathrm{sym}} = 32\,\mathrm{MeV}$. V_{c} is the Coulomb potential and U_{Yuk} is the Yukawa (surface) potential, which has the following form:

$$\begin{aligned} U^{\mathrm{Yuk}} = {} & \frac{V_{\mathrm{y}}}{2m}\sum_{i\neq j}\frac{1}{r_{ij}}\exp(Lm^2) \\ & [\exp(-mr_{ij})\mathrm{erf}(\sqrt{\mathrm{L}}\mathrm{m} - \mathrm{r_{ij}}/\sqrt{4\mathrm{L}}) \\ & - \exp(mr_{ij})\mathrm{erf}(\sqrt{\mathrm{L}}\mathrm{m} + \mathrm{r_{ij}}/\sqrt{4\mathrm{L}})] \end{aligned} \quad (3)$$

with $V_{\mathrm{y}} = 0.0074\,\mathrm{GeV}$, $m = 1.25\,\mathrm{fm}^{-1}$, $L = 2.16\,\mathrm{fm}^2$, and the relative distance $r_{ij} = |\vec{r}_i - \vec{r}_j|$. In the model, the radial density can be written as:

$$\begin{aligned} \rho(r) = {} & \sum_i \frac{1}{(2\pi L)^{3/2}}\exp\left(-\frac{r^2+r_i^2}{2L}\right)\frac{L}{2rr_i} \\ & \times\left[\exp\left(\frac{rr_i}{L}\right) - \exp\left(-\frac{rr_i}{L}\right)\right] \end{aligned} \quad (4)$$

with the summation of all nucleons.

In the IQMD model, clusters emitted in a collision are usually distinguished using the coalescence method in which nucleons with relative spatial distance Δr smaller than 3.5 fm and relative momentum difference Δp smaller than $300\,\mathrm{MeV}/c$ are treated as part of a cluster [22, 25, 26]. There are other different clustering methods that may change the fragment production rate, but the ratios of $R(n/p)$ and $R(t/^3\mathrm{He})$ are only slightly affected by clustering methods and other effects [27].

The nucleon–nucleon (NN) cross section used in the model is an experimental parameterization, which is also isospin-dependent. The cross section between neutron and proton is about three times larger than that between neutron and neutron, or proton and proton, when the collision energy is below 300 MeV/u.

For the initialization of the nucleons of the projectile and target, the IQMD model distinguishes between proton and neutron. The neutron and proton density distributions of the projectile and the target nuclei are determined by the SHF theory, with the so-called SkM* parameters. The stability of the initialized phase space of the projectile and the target is checked by the time evolution in the mean field until 200 fm/c according to the density distributions of the neutron and proton, rms radii, and the average binding energy. The calculated ΔR_{np} of ^{42,44,46,48,50,52,54,56}Ca isotopes are 0.019, 0.075, 0.124, 0.167, 0.242, 0.301, 0.357, and 0.401 fm, respectively.

3 Results and discussion

The total centrality of collisions of $^{42,44,46,48,50,52,54,56}\mathrm{Ca} + {}^{40}\mathrm{Ca}$ at 50 MeV/u is simulated by the IQMD model with soft EOS. The reduced impact parameter is used to describe the centrality of the collision as $b_{re} = b/b_{max}$, where b_{max} is the total of the radii of the projectile and target nuclei. In this study, the physical information of the fragments is carried out in the center-of-mass frame and limited at projectile-like midrapidity: the reduced rapidity in the center-of-mass frame ($y = (y/y_p)_{c.m.}$, where y_p is the rapidity of the projectile) between 0 and 0.5.

First, the time evolution of the yield ratios of $R(n/p)$ and $R(t/^3\mathrm{He})$, from $^{42}\mathrm{Ca} + {}^{40}\mathrm{Ca}$ as an example, is investigated as shown in the upper and lower panels of Fig. 1. It shows that the yield ratios of neutron to proton from midrapidity in all centralities are stable after 160 fm/c, while $R(t/^3\mathrm{He})$ becomes saturated much earlier at 140 fm/c. To improve the statistics, we accumulated the studied fragments from 180 to 200 fm/c. It appears that the larger the impact parameter, the greater the ratios, which may be because the main difference between neutron and proton density distribution lies in the surface of the nucleus.

To compare the reduced impact parameter dependence for different Ca isotopes, Fig. 2 is plotted. It shows that the yield ratios from all the neutron-rich Ca isotope-induced reactions increase with reduced impact parameter, and the ratios from heavier Ca isotopes are larger and increase more obviously with b_{re}, especially in peripheral collisions which may be due to the greater impact of the neutron skin on larger collision parameters. For a certain Ca isotope, $R(t/^3\mathrm{He})$ is greater than $R(n/p)$ and appears to more clearly increase with b_{re} than $R(n/p)$. The yield ratios from different centrality in projectile-like midrapidities that carry the neutron–proton composition information of the projectile are close to the N/Z value of the projectile. It appears that on average, $R(n/p)$ is lower, while $R(t/^3\mathrm{He})$ is larger than the projectile's constituent N/Z value, which is consistent with the experimental result [28]. That means the

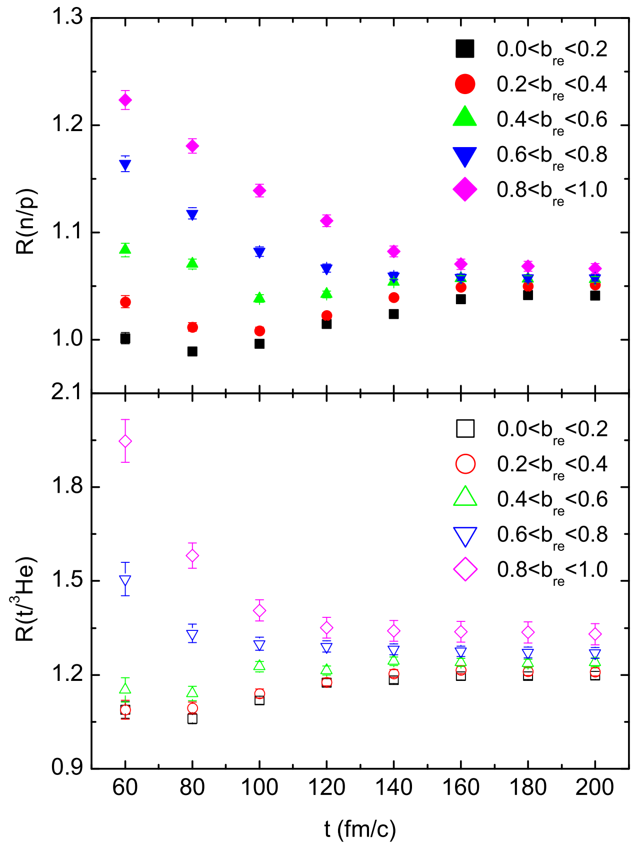

Fig. 1 (Color online) Time evolution of the yield ratios of $R(n/p)$ (solid symbols) and $R(t/^3\mathrm{He})$ (open symbols) with $0<y<0.5$ from $^{42}\mathrm{Ca} + {}^{40}\mathrm{Ca}$ at 50 MeV/u. The different symbols represent the ratios from different centralities: squares represent $0<b_{re}<0.2$, circles represent $0.2<b_{re}<0.4$, up triangles represent $0.4<b_{re}<0.6$, down triangles represent $0.6<b_{re}<0.8$, and diamonds represent $0.8<b_{re}<1$

midrapidity projectile-like fragments prefer more neutrons to protons mainly due to Coulomb repulsion and the neutron-rich circumstance. Figure 3 is plotted to examine the relationship between the yield ratios and the N/Z of the projectiles at different centralities. Strong linear correlations between $R(n/p)$, $R(t/^3\mathrm{He})$, and N/Z are exhibited for all centralities, among which the ratio values and the slopes of the correlation are the largest for peripheral collisions. This may indicate that the reaction mechanism is the same at the same reduced impact parameter for the projectiles with different N/Z induced collisions.

The corresponding neutron skin thickness dependence is shown in Fig. 4. It shows that the similar strong linear correlations between $R(n/p)$, $R(t/^3\mathrm{He})$ and neutron skin thickness are exhibited for different centralities. It may be understood that the fragments within projectile-like midrapidities are emitted from the projectile part of the collision overlap zone; thus, the yield ratios of n/p and $t/^3\mathrm{He}$ are close to N/Z of the projectile. Meanwhile, the

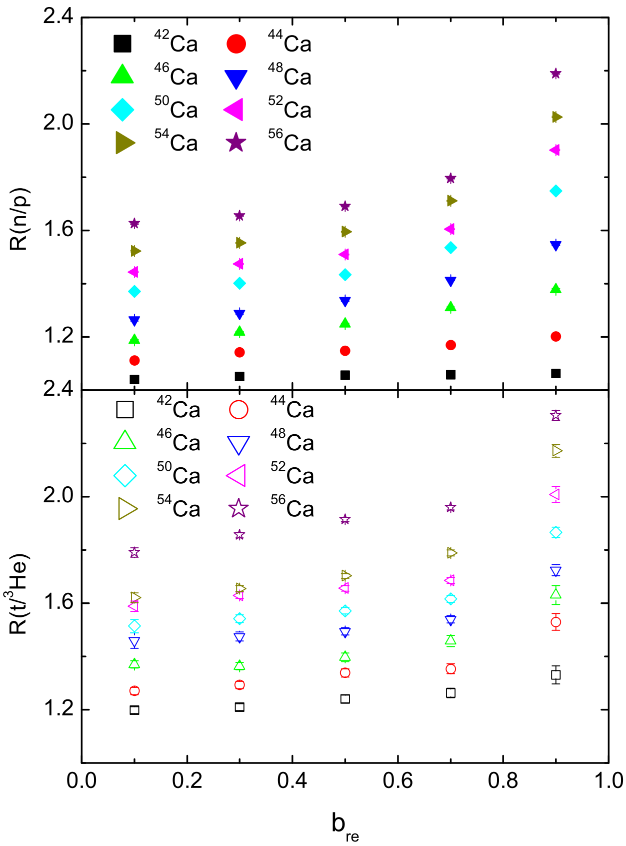

Fig. 2 (Color online) The reduced impact parameter dependence of the yield ratios of $R(n/p)$ (solid symbols) and $R(t/^3\mathrm{He})$ (open symbols) with $0<y<0.5$ from $^{42,44,46,48,50,52,54,56}\mathrm{Ca} + {}^{40}\mathrm{Ca}$ at 50 MeV/u. The different symbols represent the ratios from different projectile-induced collisions

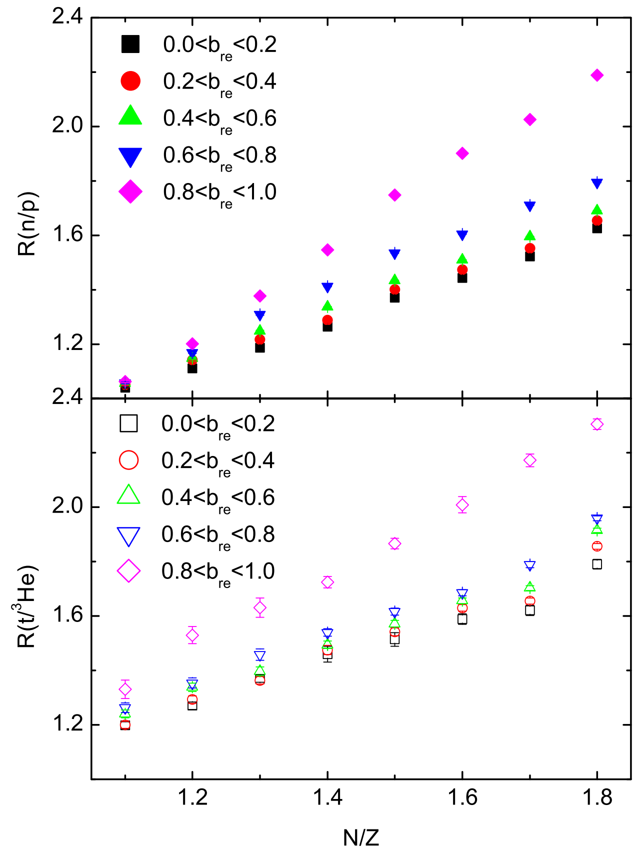

Fig. 3 (Color online) The projectile's *N*/*Z* dependence of the yield ratios of $R(n/p)$ (solid symbols) and $R(t/^3\mathrm{He})$ (open symbols) with $0<y<0.5$ from $^{42,44,46,48,50,52,54,56}\mathrm{Ca} + {}^{40}\mathrm{Ca}$ at 50 MeV/u. The different symbols represent the ratios from different centrality collisions. The dotted lines are linear fitting

neutron skin thickness should be larger for nuclei with more neutrons of the same isotope, and the yield ratios of n/p and t/3He from nuclei with larger neutron skin thickness should be larger. Therefore, one can deduce the neutron skin thickness of the projectile in an isotope chain through the detection of the midrapidity yield ratios of $R(n/p)$ or $R(t/^3\mathrm{He})$ from other isotope-induced reactions at the same reduced impact parameter, especially at peripheral collisions with larger yield ratios. The double ratios $R(t/^3\mathrm{He})/R(n/p)$ dependent on the neutron skin thickness of $^{42,44,46,48,50,52,54,56}\mathrm{Ca}$ are plotted in Fig. 5. It shows that the double ratios from different centralities are nearly equal for a certain Ca projectile and decrease very slightly with the increasing neutron skin thickness, which may be due to the relatively larger free neutron–proton ratio for the more neutron-rich projectile. In other words, $R(t/^3\mathrm{He})$ is almost proportional to the $R(n/p)$ at all centralities for different Ca isotopes, and hence $R(t/^3\mathrm{He})$ is a good replacement for $R(n/p)$ because the charged fragments of triton and ^{3}He are more easily measured than neutrons. Some model parameter dependence is investigated in the relationship between the yield ratios and the neutron skin thickness. A small change in the width of the Gaussian wave packet and the hard or soft nuclear EOS can affect the yields of the studied fragments, but almost does not change the yield ratios of $R(n/p)$ or $R(t/^3\mathrm{He})$, nor the linear relation between the yield ratios and the neutron skin thickness.

4 Summary

We simulated 50 MeV/u $^{42,44,46,48,50,52,54,56}\mathrm{Ca} + {}^{40}\mathrm{Ca}$ collisions using the IQMD model in which the initial neutron and proton densities were sampled using the SHF model, and the yield ratios of neutron to proton and ^{3}H to ^{3}He within projectile-like midrapidity were extracted. It was found that the ratios $R(n/p)$ and $R(t/^3\mathrm{He})$ from the same centrality are strongly linear with *N*/*Z* and the neutron skin thickness of the neutron-rich Ca isotopic projectiles. Moreover, the largest ratios and slopes of the linear fitting are obtained for peripheral collisions. Thus, $R(n/p)$ and $R(t/^3\mathrm{He})$ could be proposed as experimental observables

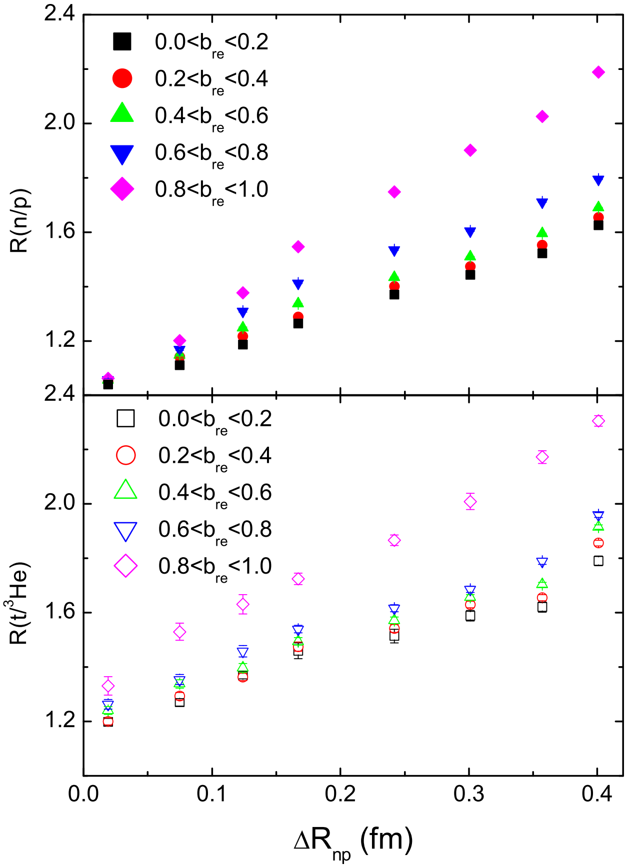

Fig. 4 (Color online) Similar to Fig. 3, but for ΔR_{np} dependence

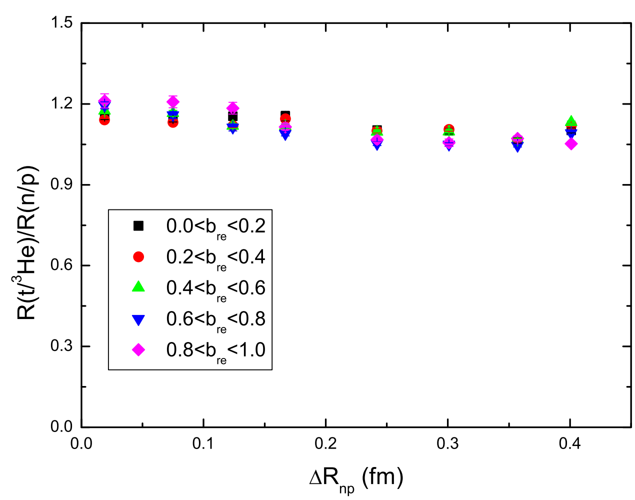

Fig. 5 (Color online) Double ratio $R(t/^{3}\mathrm{He})/R(n/p)$ with $0<y<0.5$ as a function of ΔR_{np} from $^{42,44,46,48,50,52,54,56}\mathrm{Ca}+{}^{40}\mathrm{Ca}$ at 50 MeV/u. The different symbols represent the ratios from different centrality collisions

of the neutron skin or halo thickness ΔR_{np} of neutron-rich nuclei, and we can deduce the ΔR_{np} for the nuclei near the neutron drip line through the measurement of $R(n/p)$ or $R(t/^{3}\mathrm{He})$ from isotopic nuclei near the beta-stable line. Furthermore, more information on the nuclear EOS, especially the symmetry energy at subsaturation densities, could in turn be deduced from neutron skin thickness. We recommend that a related experimental study should be conducted.

References

1. J.M. Lattimer, M. Prakash, The physics of neutron stars. Science **304**, 536 (2004). https://doi.org/10.1126/science.1090720
2. A.W. Steiner, M. Prakash, J.M. Lattimer et al., Isospin asymmetry in nuclei and neutron stars. Phys. Rep. **411**, 325 (2005). https://doi.org/10.1016/j.physrep.2005.02.004
3. P. Russotto, M.D. Cozma, A.L. Févre et al., Flow probe of symmetry energy in relativistic heavy-ion reactions. Eur. Phys. J. A **50**, 38 (2014). https://doi.org/10.1140/epja/i2014-14038-5
4. Z. Kohley, S.J. Yennello, Heavy-ion collisions: direct and indirect probes of the density and temperature dependence of E_{sym}. Eur. Phys. J. A **50**, 31 (2014). https://doi.org/10.1140/epja/i2014-14031-0
5. F. Gagnon-Moisan, E. Galichet, M.-F. Rivet et al., New isospin effects in central heavy-ion collisions at Fermi energies. Phys. Rev. C **86**, 044617 (2012). https://doi.org/10.1103/PhysRevC.86.044617
6. F.F. Duan, X.Q. Liu, W.P. Lin et al., Investigation on symmetry and characteristic properties of the fragmenting source in heavy-ion reactions through reconstructed primary isotope yields. Nucl. Sci. Tech. **27**, 131 (2016). https://doi.org/10.1007/s41365-016-0138-y
7. B.A. Li, C.M. Ko, Z.Z. Ren, Equation of state of asymmetric nuclear matter and collisions of neutron-rich nuclei. Phys. Rev. Lett. **78**, 1644 (1997). https://doi.org/10.1103/PhysRevLett.78.1644
8. J.Y. Liu, Q. Zhao, S.Q. Wang et al., Entrance channel dependence and isospin dependence of preequilibrium nucleon emission in intermediate energy heavy ion collisions. Nucl. Phys. A **687**, 475 (2001). https://doi.org/10.1016/S0375-9474(00)00581-9
9. X.G. Cao, J.G. Chen, Y.G. Ma et al., Density effect of the neutron halo nucleus induced reactions in intermediate energy heavy ion collisions. Chin. Phys. C **33**, 49–51 (2009). https://doi.org/10.1088/1674-1137/33/S1/016
10. L.W. Chen, C.M. Ko, B.A. Li, Effects of momentum-dependent nuclear potential on two-nucleon correlation functions and light cluster production in intermediate energy heavy-ion collisions. Phys. Rev. C **69**, 054606 (2004). https://doi.org/10.1103/PhysRevC.69.054606
11. L. Shi, P. Danielewicz, Nuclear isospin diffusivity. Phys. Rev. C **68**, 064604 (2003). https://doi.org/10.1103/PhysRevC.68.064604
12. H.S. Xu, M.B. Tsang, T.X. Liu et al., Nuclear isospin diffusivity. Phys. Rev. Lett. **85**, 716 (2000). https://doi.org/10.1103/PhysRevLett.85.716
13. D.Q. Fang, Y.G. Ma, C. Zhong et al., Systematic study of isoscaling behavior in projectile fragmentation by the statistical abrasion–ablation model. J. Phys. G: Nucl. Part. Phys. **34**, 2173 (2007). https://doi.org/10.1088/0954-3899/34/10/007
14. C.W. Ma, H.L. Wei, Y.G. Ma, Neutron-skin effects in isobaric yield ratios for mirror nuclei in a statistical abrasion–ablation model. Phys. Rev. C **88**, 044612 (2013). https://doi.org/10.1103/PhysRevC.88.044612
15. B.A. Li, A.T. Sustich, B. Zhang, Proton differential elliptic flow and the isospin dependence of the nuclear equation of state. Phys.

Rev. C **64**, 054604 (2001). https://doi.org/10.1103/PhysRevC.64.054604

16. M.D. Cozma, Neutron–proton elliptic flow difference as a probe for the high density dependence of the symmetry energy. Phys. Lett. B **700**, 139–144 (2011). https://doi.org/10.1016/j.physletb.2011.05.002
17. X.F. Li, D.Q. Fang, Y.G. Ma, Determination of the neutron skin thickness from interaction cross section and charge changing cross section for B, C, N, O, F isotopes. Nucl. Sci. Tech. **27**, 71 (2016). https://doi.org/10.1007/s41365-016-0064-z
18. X.G. Cao, X.Z. Cai, Y.G. Ma et al., Nucleon–nucleon momentum-correlation function as a probe of the density distribution of valence neutrons in neutron-rich nuclei. Phys. Rev. C **86**, 044620 (2012). https://doi.org/10.1103/PhysRevC.86.044620
19. N. Wan, C. Chang, Z.Z. Ren, Exploring the sensitivity of α-decay half-life to neutron skin thickness for nuclei around ^{208}Pb. Nucl. Sci. Tech. **28**, 22 (2017). https://doi.org/10.1007/s41365-016-0174-7
20. X.Y. Sun, D.Q. Fang, Y.G. Ma et al., Neutron/proton ratio of nucleon emissions as a probe of neutron skin. Phys. Lett. B **682**, 396–400 (2010). https://doi.org/10.1016/j.physletb.2009.11.031
21. Z.T. Dai, D.Q. Fang, Y.G. Ma et al., Triton/^{3}He ratio as an observable for neutron-skin thickness. Phys. Rev. C **89**, 014613 (2014). https://doi.org/10.1103/PhysRevC.89.014613
22. J. Aichelin, “Quantum” molecular dynamics-a dynamical microscopic n-body approach to investigate fragment formation and the nuclear equation of state in heavy ion collisions. Phys. Rep. **202**, 233–360 (1991). https://doi.org/10.1016/0370-1573(91)90094-3
23. L.W. Chen, F.S. Zhang, G.M. Jin, Analysis of isospin dependence of nuclear collective flow in an isospin-dependent quantum molecular dynamics model. Phys. Rev. C **58**, 2283 (1998). https://doi.org/10.1103/PhysRevC.58.2283
24. Y.G. Ma, W.Q. Shen, Z.Y. Zhu, Collective motion of reverse-reaction system in the intermediate-energy domain via the quantum-molecular-dynamics approach. Phys. Rev. C **51**, 1029 (1995). https://doi.org/10.1103/PhysRevC.51.1029
25. Y.X. Zhang, Z.X. Li, C.S. Zhou et al., Effect of isospin-dependent cluster recognition on the observables in heavy ion collisions. Phys. Rev. C **85**, 051602(R) (2012). https://doi.org/10.1103/PhysRevC.85.051602
26. W.B. He, X.G. Cao, Y.G. Ma et al., Application of EQMD model to researches of nuclear exotic structures. Nucl. Tech. **37**, 100511 (2014). https://doi.org/10.11889/j.0253-3219.2014.hjs.37.100511. (in Chinese)
27. L.W. Chen, C.M. Ko, B.A. Li, Light clusters production as a probe to nuclear symmetry energy. Phys. Rev. C **68**, 017601 (2003). https://doi.org/10.1103/PhysRevC.68.017601
28. D. Theriault, J. Gauthier, F. Grenier et al., Neutron-to-proton ratios of quasiprojectile and midrapidity emission in the ^{64}Zn $+^{64}$ Zn reaction at 45 MeV/nucleon. Phys. Rev. C **74**, 051602(R) (2006). https://doi.org/10.1103/PhysRevC.74.051602